CORROSION OF COMMON HEAT EXCHANGER MATERIALS BY LITHIUM NITRATE TRIHYDRATE

A Thesis

by

EMILY MARIE EMMONS

Submitted to the Office of Graduate and Professional Studies of
Texas A&M University
in partial fulfillment of the requirements for the degree of

MASTER OF SCIENCE

Chair of Committee,	Patrick Shamberger
Co-Chair of Committee,	Homero Castaneda
Committee Member,	Sarbajit Banerjee
Head of Department,	Ibrahim Karaman

August 2017

Major Subject: Materials Science and Engineering

ABSTRACT

Lithium nitrate trihydrate (LNH) is promising as a thermal energy storage material with one of the largest specific and volumetric enthalpies of fusion for materials with a near-room temperature melting point. In order to integrate this material into high cooling power energy storage modules, it is necessary for heat exchanger materials to be compatible with LNH. However, understanding of corrosion of metals and polymers in high salt content solutions ($w_{H2O} < 0.50$) is relatively limited. Here, we report the effects of six month immersion corrosion studies on nine common polymeric materials and twelve metallic alloys in molten LNH along with likasite, a common nucleation agent, to determine materials compatibility and degradation mechanisms. No degradation was observed in nylon, PVC, or fluorinated polymers, nor was corrosion observed in stainless steel, nickel, or titanium alloys. Copper alloys did corrode in the LNH and likasite solution, experiencing both uniform surface corrosion and localized pitting corrosion. Aluminum alloys experienced localized corrosion with LNH, which was more severe in cases with likasite present. Thus, aluminum is not recommended as a viable option for use in this system without further investigation into possible corrosion inhibitors. Potential corrosion mechanisms are discussed, and initial results of corrosion inhibitors on the corrosion rate of aluminum in LNH are presented.

CONTRIBUTORS AND FUNDING SOURCES

I would like to thank my committee chair, Dr. Shamberger, and my committee members, Dr. Castaneda and Dr. Banerjee for their guidance and support throughout the course of this research.

I would like to thank Heidi Clark for assisting in obtaining profilometry data, Yijia Zhang for assistance in collecting SEM images and EDS spectra, and Adam McClellan for assisting in setting up experiments.

This work was supported by the Raytheon Corporation [M1503262, M1700988].

TABLE OF CONTENTS

Page

LIST OF FIGURES

Page

LIST OF TABLES

Page

CHAPTER I

INTRODUCTION AND LITERATURE REVIEW

Capture, storage, and conversion of thermal energy is a critical component of efficient energy utilization as well as device or system level thermal management. Thermal energy storage (TES) systems capture excess heat during periods of high transient heat loads, and release heat during periods of low heat generation in a passive, reversible fashion [1-3]. By absorbing heat, TES devices are able to regulate the temperature of electrical, optical, and mechanical components, which prolongs device lifespan and maintains constant operating performance. TES materials presently have commercial applications in building materials (drywall), solar heat storage, HVAC systems, and in household appliances such as dishwashers, allowing for improved energy efficiency, as well as reducing the demand on the power grid during peak load times [3-5]. TES is also of interest for certain transportation applications within the aerospace sector, where performance and weight/volume considerations are of paramount importance [1, 2, 6, 7].

Phase change materials (PCMs) absorb heat associated with a physical phase transformation (melting, evaporation), and reversibly release thermal energy as they return to the original phase. Salt hydrates, one particular class of PCMs, are of particular interest for mobile use in thermal energy storage applications, due to the high specific and volumetric energy density, as well as their relatively large thermal conductivity [8-10]. Two of the key factors limiting widespread implementation of these materials are

the limited reversibility of the phase change due to super-cooling, and the corrosive effects of the salt hydrate on certain container materials. These limitations can be mitigated by including a nucleating agent so super-cooling does not occur, and selecting compatible materials to avoid any negative interactions.

Lithium nitrate trihydrate ($LiNO_3 \cdot 3H_2O$; LNH) is a promising PCM with a melting temperature of 30.1 ±0.2 °C and an enthalpy of fusion of 287 ±7 $J \cdot g^{-1}$ [9]. Multiple nucleating agents have been identified which mitigate super-cooling issues making LNH more practical for implementation in a TES system. The copper-based compound likasite, $Cu_3(NO_3)(OH)_5 \cdot 2(H_2O)$, provides LNH with a surface with similar crystal lattice parameters to initiate nucleation and reduces super-cooling in LNH to approximately 6.3 °C whereas the neat solution can suffer from a maximum super-cooling of ~70 °C [11]. A structurally related zinc hydroxy nitrate nucleating agent was also developed under NASA efforts, and while not as effective at limiting super-cooling as likasite, was able to reduce super-cooling to approximately 8 °C [11, 12]. In order to utilize LNH in TES systems, it must be contained in a hermetically sealed module as LNH is highly hygroscopic. The materials used in this container must be compatible with LNH to avoid long term degradation of the PCM, or of the container itself; it must also allow for the rapid transfer of heat to accommodate the large cooling power of LNH.

Materials used in heat exchanger assemblies should be able to rapidly conduct heat from a heat transfer fluid, or directly from a device, into a PCM, and therefore should have high thermal conductivity (k). Heat exchanger assemblies intended for

mobile use should be constructed of lightweight material to minimize the overall weight of the system, which would be reflected by materials with a low density (ρ). Considering a geometry consisting of thin fins to transfer heat into a PCM, materials with a large k/ρ transport the most heat per unit mass (Figure 1) [13]. The heat exchanger must also be resistant to corrosion to avoid degradation of the heat exchanger over its operational lifespan. Generally, these characteristics are present in a variety of metals which may potentially be utilized in the building of the heat exchanger.

In previous studies, many salt hydrates, including LNH, have been shown to be corrosive to various metals (Table 1) [1, 14-20]. In general, stainless steels are resistant to corrosion in salt hydrate solution, while carbon steel corrodes severely in such solutions. Aluminum and copper alloys are generally corroded in salt hydrate solutions, but are resistant to corrosion under some conditions. Both copper and aluminum undergo severe corrosion in hydroxide solutions which are strongly basic. However, certain copper alloys are resistant in chloride solutions, while some aluminum alloys are compatible with acetic acid solution.

Table 1 shows conflicting results for some materials which may be due to different, unspecified, alloys being tested. In the case of LNH, aluminum has shown conflicting corrosion results. One study reports Al 1016 being severely corroded while two other studies report an unspecified aluminum alloy as not being corroded [1, 14, 15]. Previous studies also report that an unspecified copper alloy is corroded in LNH while a stainless steel and a titanium alloy were not affected [15]. For integration of LNH into a heat exchanger, it is of interest to examine interactions between this material and various

metals and alloys which have some corrosion resistant properties [14, 21]. Furthermore, as various gaskets and o-rings are potentially used in the construction of heat exchangers and could come into contact with the PCMs, it is also important to consider the compatibility of these materials with the salt hydrate.

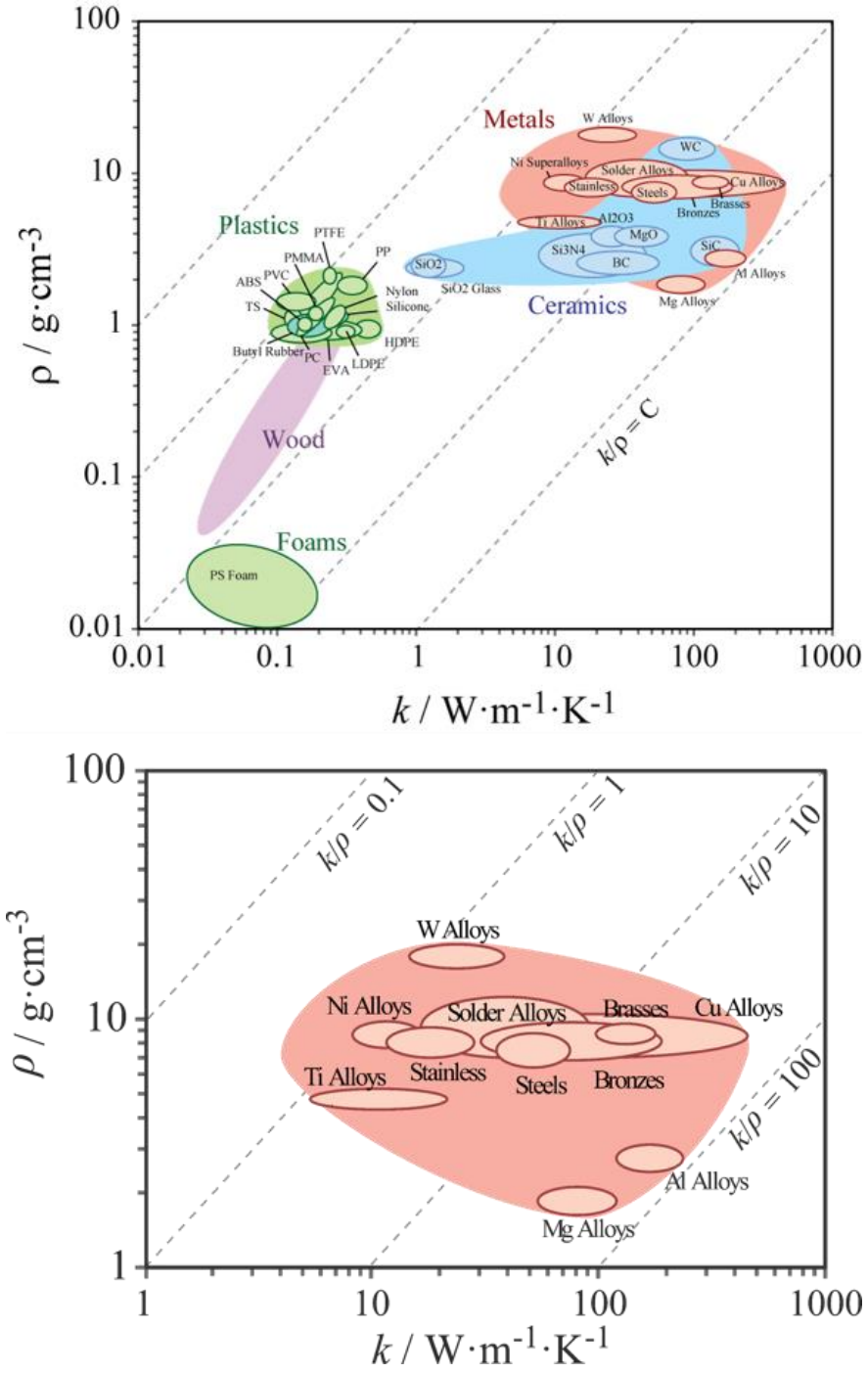

Figure 1. Density vs. thermal conductivity of a) different principal classes of materials, and b) common metals used in constructing heat exchangers. Data in this figure compiled from MatWeb [13].

Table 1. Previous Salt Hydrate Material Compatibility Study

Salt Hydrate	Aluminum Alloy	Brass Alloy	Copper Alloy	Carbon Steels	Stainless Steels	Titanium Alloy
$NaOAc{\cdot}3H_2O$	En AW-2007 + [16]	Ms58 Flach – [16]	E-Cu 57 – [16]	Mat. No. 1.0345 + [16]	Mat. No. 1.4301 + [16]	
$LiClO_3{\cdot}3H_2O$	A199wh DIN 1783 – – [17] Anodized AlMg3h DIN 1783 – [17]	Ms 63 F 38 DIN 1751 – [17]	F 20 DIN 1751 + [17]	Mild DIN 1541 – [17] Zinced DIN 1541 – – [17]	18/8 CrNiTi189 + [17]	
$CaCl_2{\cdot}6H_2O$	A199wh DIN 1783 – – [17] Anodized AlMg3h DIN 1783 – – [17] AlCuMg DIN 1798 – – [17] AlMgSi DIN 1795 – – [17] En AW-2007 – – [18] Al* – [19]	Ms 63 F 38 DIN 1751 – [17] Ms58 Flach + [18]	F 20 DIN 1751 – [17] E-Cu 57 + [18] Cu* – [19]	Mild DIN 1541 – [17] Zinced DIN 1541 – [17] Mat. No. 1.0345 – [18] Carbon Steel* – [19]	18/8 CrNiTi189 + [17] Mat. No. 1.4301 + [18] SS 316 + [19]	
$MgCl_2{\cdot}6H_2O$	Al* – [19]		Cu* – [19]	Carbon Steel* – – [19]	SS 316 + [19]	
$ZnCl_2{\cdot}3H_2O$	Al* – – [20]		Cu* + [20]	Carbon Steel* – – [20]	SS 316 + [20]	
$KF{\cdot}4H_2O$	A199wh DIN 1783 – [17] Anodized AlMg3h DIN 1783 + [17] AlCuMg DIN 1798 – [17] AlMgSi DIN 1795 + [17]	Ms 63 F 38 DIN 1751 + [17]	F 20 DIN 1751 + [17]	Mild DIN 1541 + [17] Zinced DIN 1541 – [17]	18/8 CrNiTi189 + [17]	
$Ba(HO)_2{\cdot}8H_2O$	Al* – – [1]					
$NaOH{\cdot}XH_2O$	Al* – – [20]		Cu* – – [20]	Carbon Steel* – [20]	SS 316 + [20]	

Table 1 Continued.

Salt Hydrate	Aluminum Alloy	Brass Alloy	Copper Alloy	Carbon Steels	Stainless Steels	Titanium Alloy
$LiNO_3 \cdot XH_2O$	1016 – – [14] Al* + [1] Al* + [15]		Cu* - [15]		SS* + [15]	Ti* + [15]
$Zn(NO_3)_2 \cdot XH_2O$	En AW-2007 – – [18] Al* – – [20]	Ms58 Flach – – [18]	E-Cu 57 – – [18] Cu* – – [20]	Mat. No. 1.0345 – – [18] Carbon Steel* – – [20]	Mat. No. 1.4301 + [18] SS 316 + [20]	
$K_3PO_4 \cdot 7H_2O$	Al* – – [20]		Cu* – – [20]	Carbon Steel* + [20]	SS 316 + [20]	
$K_2HPO_4 \cdot 6H_2O$	Al* – – [20]		Cu* – [20]	Carbon Steel* – – [20]	SS 316 + [20]	
$Na_2HPO_4 \cdot 12H_2O$	A199wh DIN 1783 – – [17] Anodized AlMg3h DIN 1783 – – [17] AlCuMg DIN 1798 – – [17] AlMgSi DIN 1795 – – [17] En AW-2007 – – [18] Al* – – [1]	Ms 63 F 38 DIN 1751 – [17] Ms58 Flach + [18]	F 20 DIN 1751 – [17] E-Cu 57 – [18]	Mild DIN 1541 + [17] Zinced DIN 1541 – – [17] Mat. No. 1.0345 – [18]	18/8 CrNiTi189 + [17] Mat. No. 1.4301 + [18]	
$MgSO_4 \cdot 7H_2O$	Al* – [19] Al* + [20]		Cu* – – [19] Cu* – [20]	Carbon Steel* – – [19] Carbon Steel* – – [20]	SS 316 + [19] SS 316 + [20]	
$Na_2S \cdot 5H_2O$	Al* – – [19]		Cu* – – [19]	Carbon Steel* – [19]	SS 316 + [19]	
$Na_2S_2O_3 \cdot 5H_2O$	En AW-2007 + [16] Al* – [20]	Ms58 Flach – – [16]	E-Cu 57 – – [16] Cu* – – [20]	Mat. No. 1.0345 + [16] Carbon Steel – [20]	Mat. No. 1.4301 + [16] SS 316 + [20]	

+ = no significant corrosion
– = some corrosion occurs
– – = severe corrosion
** unspecified purity*

CHAPTER II

DEGREDATION OF METALS AND POLYMERS BY LITHIUM NITRATE TRIHYDRATE

II.1 Introduction

While observations of corrosion rates and mechanisms are relatively abundant for aqueous saline solutions, very limited information is available on these processes at the high salt concentrations (> 50 wt% salt) which characterize most salt hydrates. In this study, we investigate the corrosion of 12 alloys (including aluminum-, copper-, nickel-, and titanium-based alloys, and stainless steels). These alloys have been selected for two criteria: 1) large k/ρ, and 2) likely resistance to corrosive effects of liquid lithium nitrate trihydrate. Furthermore, we also investigate the degradation of 9 polymeric materials, representing a range of gasket, flange, and rigid plastic structural components. In this study, both metals and polymers were immersed in liquid LNH in the presence of (and in some cases the absence of) a nucleation agent, likasite, for a period of six months at 50 °C. At the end of the study, samples were evaluated for mass loss or gain, and local pitting densities and characteristics. Corrosion rates are evaluated, and corrosion mechanisms are discussed.

II.2 Materials and Methods

II.2.1 Material Synthesis and Preparation

As-received reagent grade anhydrous $LiNO_3$ (Sigma-Aldrich, >95% purity) was dried at 150 °C for 6 hours under vacuum to remove residual moisture. Anhydrous $LiNO_3$ was combined with deionized (DI) water in a mass ratio of 1:0.784 ($LiNO_3$: H_2O). To ensure the salt hydrate was homogeneous, the container of lithium nitrate trihydrate (LNH; $LiNO_3 \cdot 3H_2O$) was placed in a 75 °C water bath and agitated periodically for a period of at least an hour. After preparation, bottles were capped, and sealed with an additional paraffin film layer, to minimize exposure to the atmosphere, as LNH is hygroscopic. Thermal properties were measured by differential scanning calorimetry (DSC) to confirm the composition of LNH, as the behavior of the melting peak is very sensitive to water content. The fusion temperature, $T_{fus,}$ is within 1%, and the enthalpy of fusion, ΔH_{fus}, is within 5% of previously reported values (30.1 ± 0.3 °C, 287 ± 14 J/g, respectively) [9].

Likasite, $Cu_3(NO_3)(OH)_5 \cdot 2H_2O$, is precipitated from a basic solution of copper (II) acetate (Sigma-Aldrich, 98% purity), sodium nitrate (Sigma-Aldrich, >99% purity), and sodium hydroxide (Sigma-Aldrich, >98% purity) following the procedure described by Yoder *et al* [22]. The resulting powder is observed to be a light powder blue color, and its activity as a nucleation catalyst was confirmed through DSC crystallization experiments. Likasite was added to aging samples and test samples in concentrations of 0.05 wt% (+/- 0.01 wt%).

Following ASTM G1-03(2011), material test coupons and o-rings, which can be found in Table 2 and Table 3, were washed in a soapy water solution, then rinsed using DI water, and dried in a 70 °C oven for 1 hour. The mass (+/- 0.1 mg), using an Ohaus Explorer EX225D balance, and dimensions (+/- 0.1 mm), using digital calipers, of each material sample were measured and recorded.

II.2.2 Immersion Aging

LNH solutions were solidified and the headspace of containers was reduced to <1 v. % air by flow-through purge in a dry box with high purity nitrogen (99.999 %). The salts were then melted and re-solidified to reduce dissolved gas and the headspace was once again reduced to <1 v. % air using high purity dry nitrogen. To prepare sample vials, a glove box was purged to <0.1 v. % air using high purity nitrogen. Following ASTM G31-12a, material samples were placed in borosilicate glass vials and the liquid LNH with likasite was added to each vial to fully submerge the samples (~9 mL). Some of the non-metal o-rings (EPDM, Nylon, BNR, and VMQ) were buoyant in solution, so all vials containing o-rings were filled with ~5 mL of the melted salt with likasite. The PVC and PC were also somewhat buoyant, but remained immersed completely in the solution when the vial was filled to ~ 9 mL. Due to an anticipated reaction between likasite and aluminum, additional samples of the aluminum alloys were tested in neat LNH (without any likasite added). Vials were capped with a small amount of vacuum grease to prevent gas exchange prior to removing from the glove box. Aging was carried out in an oven at 50 °C for a period of 6 months.

Table 2. Composition and Source of Alloys Used in Immersion Study.

ID	Common Name	UNS	Composition [a] (wt%)	Producer
Copper Alloys				
Cu1	Cu C11000	C11000	>99.90 Cu	Revere Copper Products, Inc
Cu2	Cu-Ni 70/30	C71500	69.5 Cu, 29.0-33.3 Ni (+ Fe)	Hussey Copper
Aluminum Alloys				
Al1	Al 1100-H18	A91100	>99.0 Al (+ Cu)	Reynolds Metal Supply Company
Al2	Al 6061-T6	A96061	95.8-98.6 Al (+ Cr, Cu, Mg, Si)	Skana Aluminum Company
Al3	Al 4047	A94047	88 Al-12 Si (<0.8 Fe)	Eagle Alloys
Stainless Steels				
SS1	SS 316L	S31603	69 Fe, 17 Cr, 12 Ni, 2 Mo	Outokumpu
SS2	SS 2205	S31803	69.5 Fe, 22 Cr, 5.5 Ni, 3 Mo	Outokumpu
SS3	Al-6XN	N08367	48 Fe, 21 Cr, 24.5 Ni, 6.5 Mo	Rolled Alloys
Nickel Alloys				
Ni1	C-276	N10276	59.5 Ni, 15.5 Cr, 16 Mo, 5 Fe, 4 W	Haynes International
Titanium Alloys				
Ti1	CP Ti Grade 4	R50700	98.6+ Ti (<0.4 O, <0.5 Fe)	RMI Titanium
Ti2	Ti Grade 5	R56400	90 Ti, 6 Al, 4 V	Titanium Metals Corporation
Ti3	TiBraze 200		40 Ti, 20 Zr, 20 Cu, 20 Ni	Titanium Brazing Inc.

[a] Compositions defined by ASTM guidelines

Table 3. Polymers Investigated in Immersion Study

Composition	Sample ID
Ethylene-propylene-diene Rubber	EPDM
Nylon	Nylon
Acrylonitrile-butadiene rubber (Nitrile Rubber)	BNR
Polysiloxane (Silicone Rubber)	VMQ
Hexafluoropropylene-vinylidene fluoride (Fluorocarbon Rubber)	FKM
Polytetrafluoroethylene	PTFE
Fluorosilicone Rubber	FVMQ
Polyvinyl chloride	PVC
Polycarbonate	PC

All samples were immediately and thoroughly rinsed in DI water after removal from LNH and allowed to dry. Corrosion rates of metals were determined after removal of corrosion products on aluminum and copper samples according to ASTM G1-03. Aluminum alloys were cleaned by immersing the sample in concentrated nitric acid (sp. gr. 1.42) for 90-120 seconds at room temperature. Copper alloys were immersed in a hydrochloric acid solution composed of 50 v. % hydrochloric acid (sp. gr. 1.19) and 50 v. % DI water for 90-120 seconds. After removal from the acid baths, metal samples were rinsed, sonicated in DI water, and brushed with a non-metallic brush to ensure the removal of corrosion products. Mass loss of metal samples after cleaning was corrected to a reference alloy, which underwent the same cleaning procedure, to minimize error in removal of the non-corroded base metal. Other samples did not require aggressive

cleaning as there were no microscopically visible corrosion products and no significant mass change was measured.

II.2.3 Material Characterization

Scanning electron microscopy (SEM) and energy-dispersive X-ray spectroscopy (EDS) were carried out on a Tescan LYRA-3 Model GMH Focused Ion Beam Microscope. The microscope uses a Schottky Field emission electron source and SEM images were captured using a secondary electron detector and an acceleration voltage of 20 kV. EDS spectra were captured using an Oxford Instruments X-Man^{N} 50 mm^{2} silicon drift detector. Optical microscopy was carried out using an Olympus BX53M microscope equipped with an Olympus UC30 camera under bright field reflected light conditions. X-Ray diffraction measurements were carried out on a Bruker D8 Focus Bragg-Brentano X-ray powder diffractometer with Cu Kα radiation equipped with a Lynxeye 1D strip detector. The scan angle was 5 ° to 90 ° 2θ with a static stage under ambient conditions. Differential scanning calorimetry (DSC) was carried out using a TA Instruments Q2000 using N_2 flow gas at 50 mL·min^{-1} and liquid nitrogen cooling. Liquid samples of 8.5 µL were placed in aluminum pans and hermetically sealed. Scans were carried out from -35 °C to 50 °C with a ramp rate of 10 °C·min^{-1}.

II.3 Results

II.3.1 Polymers

Visual inspection of vials containing EPDM and BNR rings after six months of aging revealed a color change of the likasite in the LNH solution from blue to green,

indicating the copper ions in the likasite crystals reacted leading to a change of oxidation state, and the presence of a yellow precipitate at the bottom of the vial. After removal from solution and rinsing in DI water, EPDM and BNR o-rings were observed to have changed in color from black to light gray on the surface in contact with the LNH. No other visible changes in the polymer samples were observed.

As shown in Figure 2, select polymers experienced a significant mass loss or gain as the study was conducted. Mass change was normalized to the surface area of the polymer samples. The most significant changes in mass were observed in EPDM, BNR, and VMQ, all of which lost mass during the study, suggesting bulk degradation of these polymers in contact with LNH. In contrast, FKM samples exhibited a small mass gain throughout the course of the study suggesting swelling of FKM in LNH. The mass gain of Nylon, PTFE, and PVC are within 2σ of no mass change suggesting that these materials are highly compatible with LNH. FVMQ and PC both indicated a small, but measurable, mass gain ($< 0.3\ \mu g \cdot mm^{-2}$), suggesting that these polymers are also fairly resistant to chemical degradation by LNH solutions.

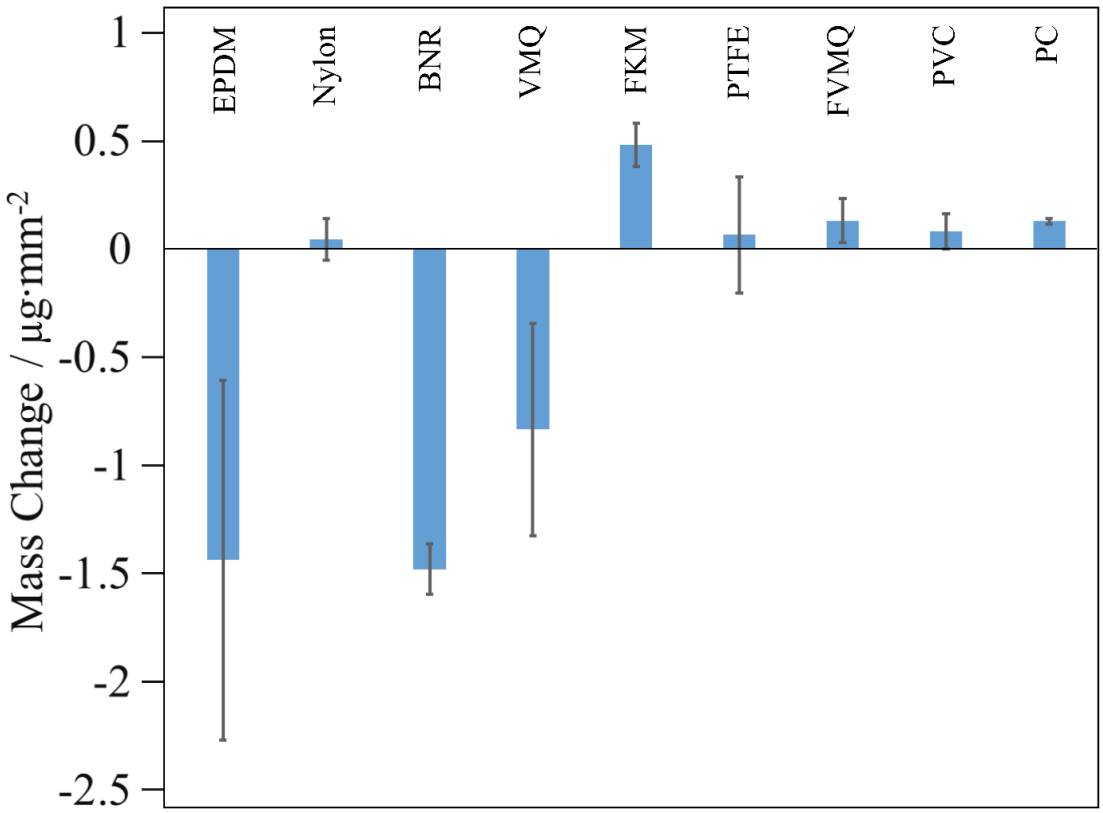

Figure 2. Mass change normalized to the surface area of polymer samples. Error bars represent 2σ, based on the analysis of 2 samples of each polymer.

II.3.2 Metals

The mass of the Cu 11000, Cu 71500, Titanium brazing alloy, Al 1100, Al 6061, and Al 4047 samples during aging increased by greater than the 2σ uncertainty of the measurement. Notably, those aluminum alloys immersed in LNH with likasite present experienced a larger increase in mass than those in a neat solution, indicating a likely reaction between the likasite and aluminum. Mass gain was recorded, and in conjunction with visible observation, was used to indicate which samples needed to undergo the

corrosion product removal process. Both the copper alloys and aluminum alloys required aggressive cleaning using acid etchants to remove corrosion products, as described in the methods section. The corrosion of Titanium alloys are reported as a mass gain by convention, as opposed to other metals which are reported as mass loss, as oxidized TiO_2 is highly resistant to corrosive etchants. The mass loss as well as the surface area of the metal samples, alloy density, and aging time were utilized to calculate the corrosion rates shown in Figure 3.

II.3.3 Localized Corrosion of Aluminum and Copper

The extent of localized corrosion pitting in aluminum alloys depends on alloy composition and strongly depends on the presence of likasite (Table 4). Al 1100 and Al 6061 alloys display more severe pitting in those samples exposed to likasite with the average density of corrosion pits an order of magnitude larger for those aluminum samples exposed to likasite. While more numerous (10^4 m^{-2} vs 10^3 m^{-2} average pit density), the pits in the cases with likasite present on average have a smaller surface area than those in the neat case (0.3 mm^2 vs 0.5 mm^2 on Al 1100). Al 4047 samples show a deviation from this behavior, with the pits being slightly less prevalent ($2.5 \cdot 10^3$ m^{-2} vs $4.9 \cdot 10^3$ m^{-2} average pit density) and much larger (3.9 mm^2 vs 0.5 mm^2) when in the presence of likasite than in the neat solution. The pits on Al 4047 with likasite present appear much deeper as a visible depression as a visible depression in the metal surface while the localized corrosion in the neat case appear more superficial and not as deep.

A limited amount of localized corrosion was also observed in the copper samples. The pits were not numerous, but had a large surface area and were

accompanied by a uniform layer of surface corrosion on the Cu11000 and Cu71500 samples.

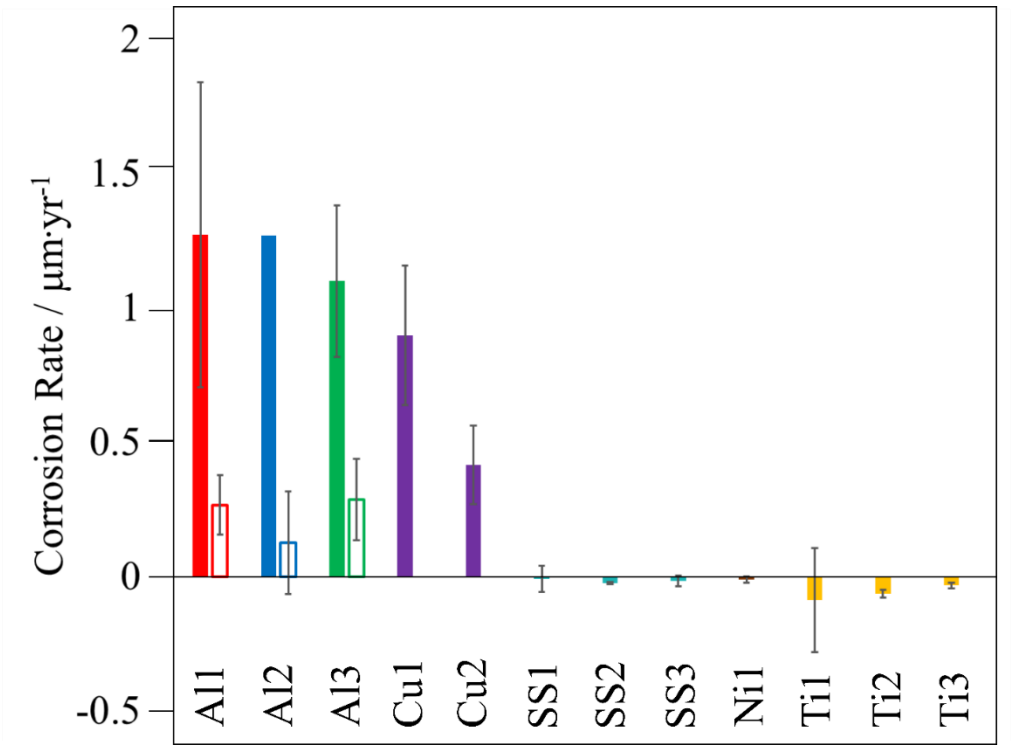

Figure 3. Corrosion rate of alloys. Error bars represent a 2σ standard deviation between samples. Solid bars represent samples with likasite present, while hollow bars are neat LNH solution. A negative quantity in this figure represents a mass gain.

Table 4. Localized Corrosion Densities and Sizes for Copper and Aluminum Alloys

		Pitting Density			Pit Surface Area			Pitting Depth		
		N_{sample}	mean/m^{-2}	2σ /m^{-2}	N_{pit}	mean/mm^2	2σ /mm^2	N_{pit}	mean/mm	2σ
Al1		2	$4.4 \cdot 10^4$	$7.03 \cdot 10^4$	87	0.3	1.0	14	46	37
	*	2	$3.5 \cdot 10^3$	$4.30 \cdot 10^4$	7	0.5	1.2	3	60	5
Al2a		1	$8.7 \cdot 10^4$	--	90	0.2	1.1	14	38	30
	*	2	$3.4 \cdot 10^3$	$1.35 \cdot 10^3$	7	0.6	1.1	4	55	23
Al3		2	$2.5 \cdot 10^3$	$1.53 \cdot 10^3$	5	3.9	6.6	4	53	10
	*	2	$4.9 \cdot 10^3$	$2.97 \cdot 10^3$	10	0.5	1.3		--	--
Cu1		2	$8.9 \cdot 10^2$	$6.8 \cdot 10^{-2}$	2	1.5	0.7	1	30	--
Cu2		2	$3.1 \cdot 10^3$	$1.25 \cdot 10^3$	7	2.5	2.9	4	13	19

* samples in neat solution

SEM and EDS were used to examine the localized corrosion spots on Al 1100 and Al 6061 to examine the corrosion products and identify atomic species are present. As mentioned previously, aluminum alloys in the presence of likasite showed frequent occurrences of localized corrosion, while those samples in neat LNH solution had less frequent localized corrosion. The SEM images of the corrosion products in both cases appear similar in morphology (Figure 4). Most notable was the EDS spectra from the samples when comparing those in the presence of likasite and those in neat solution (Figure 5). Localized corrosion spots on the samples in the presence of likasite show trace amounts of copper are present in the corrosion products.

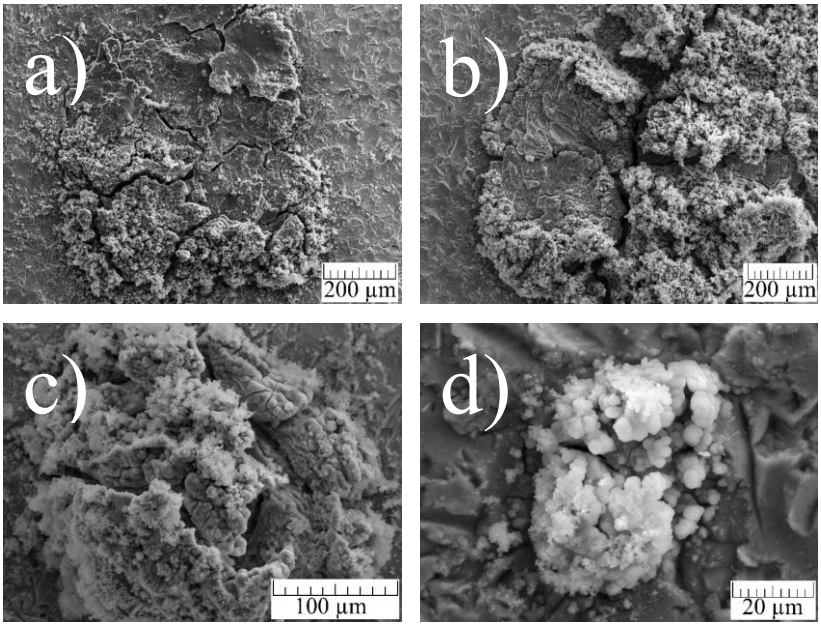

Figure 4. Corrosion products after aging a) Al 1100 in LNH with likasite, b) Al 1100 in neat LNH, c) Al 6061 in LNH with likasite, d) Al 6061 in neat LNH.

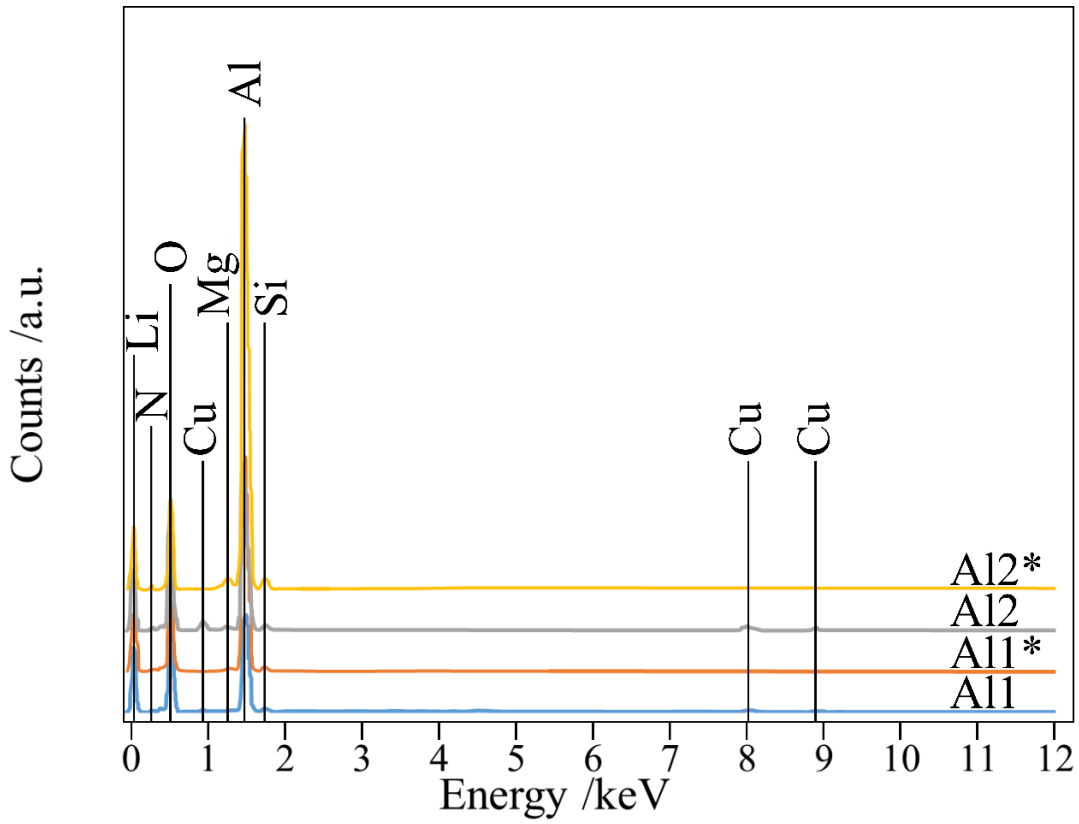

Figure 5. EDS spectra of aluminum 1100 (Al1) and 6061 (Al2) in neat LNH and in the presence of likasite. The * symbol indicates neat LNH.

The XRD spectra of the corrosion products on aluminum 1100 and 6061 samples includes peaks 10.6 ° 2θ and 20.6 ° 2θ (Figure 6), which do not correspond with the pattern for aluminum. We attribute these peaks to corrosion products on the surface. The peak near 10.6 ° 2θ corresponds to a low angle peak for $LiAl_2(OH)_7{\cdot}2H_2O$ and cannot be assigned to common aluminum oxide or hydroxide phases [11, 23]. The other peak (20.6 ° 2θ) could potentially be related to the same phase, although it also overlaps potential $Al(OH)_3$ gibbsite peaks. The stick diagrams below the scan data represent the relative

signal intensity for the species listed. Not all peaks from the candidate phases appear, which suggests significant preferred orientation in the corrosion product.

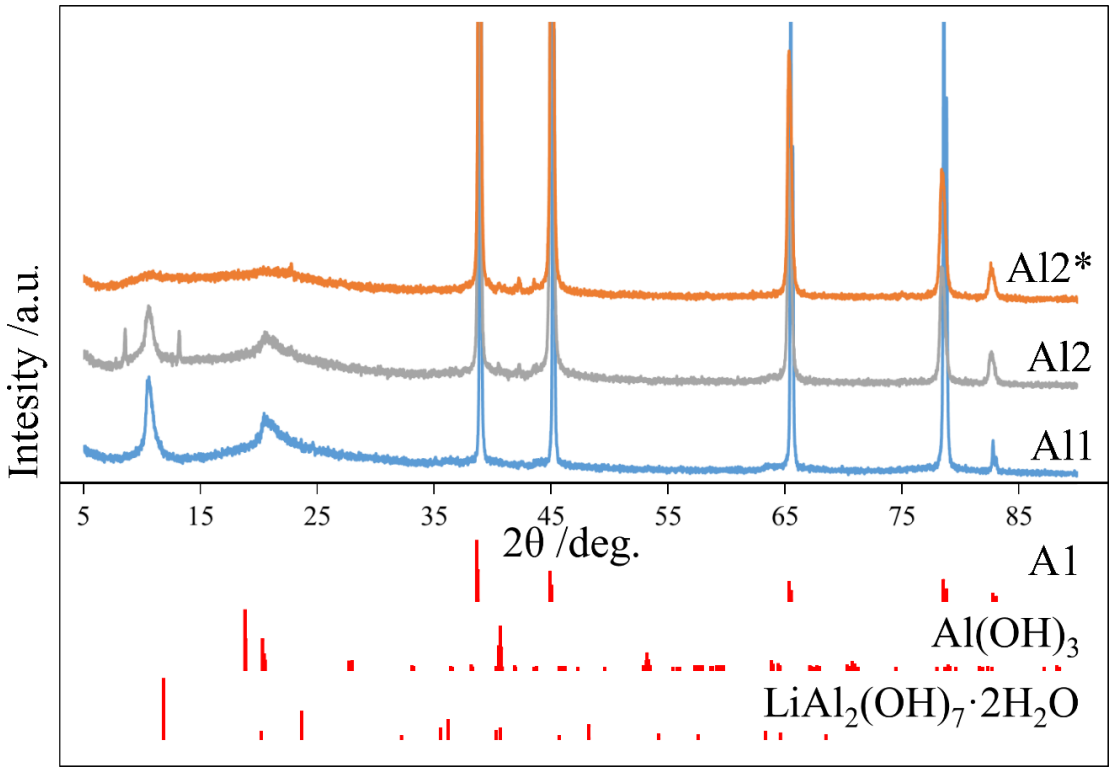

Figure 6. X-Ray diffraction pattern for corrosion products on Al 1100 (Al1) and Al 6061 (Al2). The * represents a sample aged in neat LNH. Stick diagrams below the data represent the aluminum base metal and possible corrosion products.

II.3.4 Thermal Properties of LNH after Aging

Immediately after six months of aging, the thermal properties of the LNH solutions were tested following previously described methods to determine if any

significant changes to their thermal properties occurred during the aging process (Figure 7).

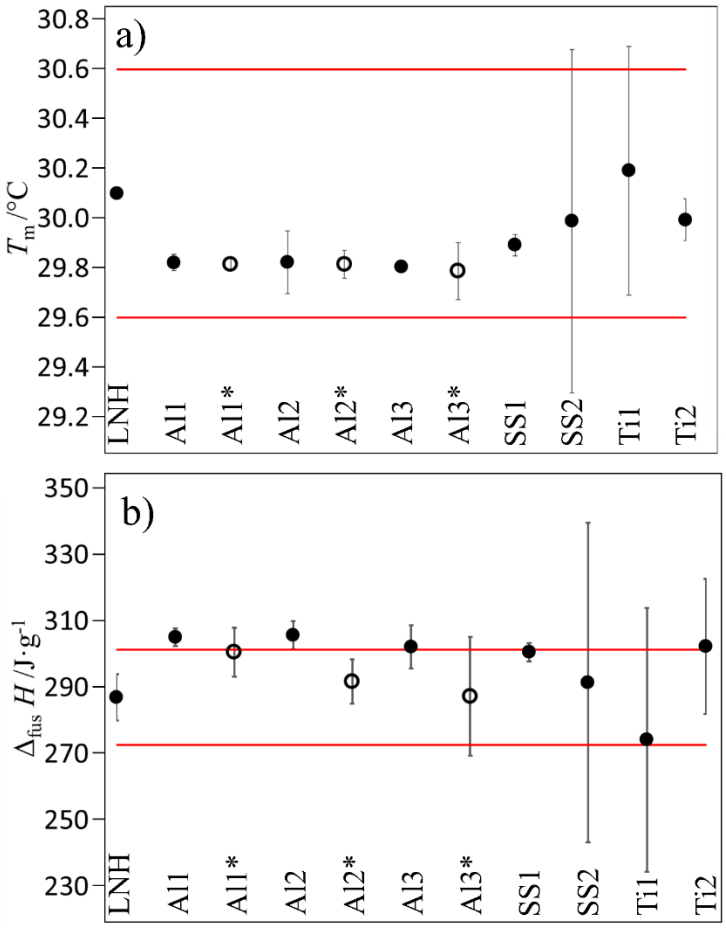

Figure 7. Thermal data for LNH solutions after aging. The * symbol indicates neat LNH. a) shows the melting temperature of LNH while b) shows the heat of fusion. Error bars represent a 2σ standard deviation between samples.

The DSC study revealed that the melting temperatures of the solutions did not change by more than 0.5 °C over the course of the study, and the heat of fusion

measurements were more varied, but tended to fall within 5 % of the accepted value for the heat of fusion of LNH [9]. These upper and lower bounds are depicted by the red horizontal lines in Figure 7.

Stainless Steel 2205 and Titanium Grade 4 have larger error bars, in both the melting temperature study and the heat of fusion study, than the other materials tested. For both of these materials, the solution in one immersion test vial had a higher than average values for T_m along with a lower than average ΔH_{fus}, while the solution in the other immersion test vial would have exhibited the opposite.

II.4 Discussion

II.4.1 Polymers

Polymers which exhibit significant mass loss during the immersion (EPDM, BNR, and VMQ) were determined to be unsuitable for long term use in LNH. This mass loss is indicative of chemical degradation occurring in the polymeric structures. The presence of a yellow precipitate in the bottom of the vials along with discolored likasite indicate that the chemical interaction involves the nucleating agent. FKM, and to a lesser degree, FVMQ and PC gained mass over the course of the experiment leading to these materials also not being recommended for long term use in contact with the LNH solution. VMQ is a silicone rubber while FVMQ is a fluorinated silicone rubber; due to the significant difference in the long term effect of exposure it is apparent that the fluorinating of the functional groups is significant when considering the possible chemical interaction of these materials with LNH. Nylon, PTFE, and PVC did not

experience significant changes in mass over the course of the study indicating that they are all compatible with LNH for long term use.

II.4.2 Metals

Corrosion rates of Aluminum and Copper alloys indicate significant corrosion when in contact with LNH solutions. However, Stainless Steel, Nickel, and Titanium alloys did not experience significant corrosion, and are therefore compatible for long term use with LNH. While these metals are compatible with these solutions, they do not have a favorable k/ρ ratio (as seen in figure 1) and would therefore not be suitable in applications which require high heat transfer rates.

It has been shown that the corrosion of aluminum in alkaline solution with sodium nitrate present follows the reactions (1) and (2) shown below with the aluminum being oxidized and nitrate being reduced [24].

$$8Al_{(s)} \leftrightharpoons 8Al^{3+} + 24e^- \quad (1)$$

$$3NO_3^- + 18H_2O + 24e^- \leftrightharpoons 3NH_3 + 27OH^- \quad (2)$$

In neutral solutions, this direct chemical dissolution cannot occur, therefore corrosion occurs through electrochemical reactions (3) through (5) [14].

$$Al + H_2O \leftrightharpoons Al(OH)_{(ads)} + H^+ + e^- \quad (3)$$

$$Al(OH)_{(ads)} + H^+ \leftrightharpoons Al^{3+} + H_2O + 2e^- \quad (4)$$

$$Al^{3+} + 3H_2O \leftrightharpoons Al(OH)_3 + 3H^+ \quad (5)$$

The pH of the LNH solutions were found to be between 3 and 3.5, and when the pH of a solution is less than 4, the protective Al_2O_3 layer commonly found on the surface of aluminum is dissolved leaving unprotected base metal to react [25]. It has been shown that in aqueous hydrochloric acid solution, the reaction mechanism follows equations (6) through (9) [26]. The electrons generated in this system are consumed in reducing hydrogen ions to hydrogen gas.

$$Al + H_2O \leftrightharpoons Al(OH)_{(ads)} + H^+ + e^- \quad (6)$$

$$Al(OH)_{(ads)} + H^+ \leftrightharpoons Al^{3+} + H_2O + 2e^- \quad (7)$$

$$Al^{3+} + H_2O \leftrightharpoons [AlOH]^{2+} + H^+ \quad (8)$$

$$[AlOH]^{2+} + Cl^- \leftrightharpoons [Al(OH)Cl]^+ \quad (9)$$

Taking this information into consideration and combining our observations via EDS and XRD, it is suggested that the reaction occurring in our system, which is acidic and has Li^+ ions present, is likely to follow the reactions (10) through (12) listed below resulting in precipitation of insoluble corrosion products $LiAl_2(OH)_7 \cdot 2H_2O$ potentially accompanied by $Al(OH)_3$. We made no observations of intermediates of this reaction but the intermediates could be as shown in (3)/(4) and (6)/(7). We are unable to determine what is being reduced in our solutions, but it is likely to be hydrogen ions reducing to hydrogen gas, or the nitrate ions may be reduced to nitrites.

$$Al_{(s)} \leftrightharpoons Al^{3+}_{(aq)} + 3e^- \quad (10)$$

$$Li^+ + 2Al^{3+} + 9H_2O \leftrightharpoons LiAl_2(OH)_7 \cdot 2H_2O + 7H^+ \quad (11)$$

$$Al^{3+} + 3\ H_2O \leftrightharpoons Al(OH)_3 \quad (12)$$

Aluminum alloys which were aged in contact with the likasite nucleating agent experienced significantly increased corrosion rates compared to those in neat solution. When the corrosion products of the aluminum samples aged in LNH with likasite present were examined using EDS, trace amounts of copper were detected. This strongly suggests that copper plays an important role in the localized corrosion reaction, but is not responsible for the bulk corrosion products. We hypothesize that despite low solubility of likasite, a small amount of the copper ions dissolve into the solution from likasite and induce galvanic corrosion in the aluminum alloys where the copper is reduced from the +2 state which it exists in likasite and the aluminum is oxidized to Al^{3+}. The electrochemical potential, which can be used to predict the direction of galvanic reactions, of copper and aluminum support this hypothesis as $E^0(V) = 0.34$ for copper and $E^0(V) = -1.66$ for aluminum with the material with the more positive value (copper) being thermodynamically driven to reduce, while the more negative (aluminum) is driven to be oxidized [25]. This reaction causes more severe damage to the aluminum samples than they experience in conditions where likasite is not present. This is also supported by the pitting data which shows the pitting density on aluminum samples is an order of magnitude higher in the Al 1100 and Al 6061 alloys, and the density doubles on the Al 4047 alloy.

Copper alloys corroded in a predictable manner, with the commercially pure Cu 11000 experiencing more severe corrosion than the alloyed Cu 71500 which has nickel present. The nickel added to the copper generally affords some degree of corrosion resistance, but in this case was not effective enough to meet the long-term compatibility requirements [27]. The corrosion resistance of alloying copper with nickel is supported by the dissolution potential in sea water near room temperature of pure copper (-360 mV) being far more active than that of Cu 71500 (-250 mV) [25]. We predict copper is corroding through concentration cell corrosion, where a gradient in copper ion concentration in the solution surrounding the sample leads to an electrochemical potential and copper ions being dissolved from one area of the sample and reduced and deposited on another area. This is the typical mechanism for copper pitting corrosion, which was observed on the samples of both Cu 11000 and Cu 71500 [27]. It is also predicted that the copper is reacting leading to the formation of copper hydroxide and copper hydroxyl nitrate as the protective copper oxide layer is not stable at pH below 5, and nitrate anions become more aggressive toward copper at low pH and high temperature [27].

The thermal study carried out on the post aging samples indicate that there was no significant change to the chemical composition of the LNH when in contact with Aluminum alloys, Stainless Steel 316L, Stainless Steel 2205, or Titanium Grade 4 or 5. The thermal properties of this material are very sensitive to changes in composition and even minor changes would result in a measurable change in melting temperature or heat

of fusion. This suggests that any possible reactions that would change the overall concentration of lithium ions from LNH are unlikely.

II.5 Conclusion

For long term use with LNH solution, any polymeric components should be composed of Nylon, PTFE, or PVC. Fluorinated polymeric materials were more resistant to degradation in LNH than non-fluorinated version. Any metallic components in long term contact with LNH solutions should be composed of Stainless Steel 316, Stainless Steel 2205, AL6XN, C-276, Titanium Grade 4, or Titanium Grade 5.

The mechanism of corrosion in the aluminum samples in neat solution likely follows a similar path to typical corrosion mechanism of aluminum in contact with neutral water or aqueous hydrochloric acid. The significant increase in the corrosion rate of aluminum when likasite was present suggested that in addition to the corrosion caused by the LNH, a galvanic coupling was formed in these cases resulting in more sever corrosion. As the aluminum alloys are of high interest for constructing heat exchangers, further studies into corrosion inhibition should be explored. Copper corrosion was likely caused by a combination of concentration cell corrosion and uniform surface corrosion caused by immersion in an acidic solution with nitrates present.

CHAPTER III

ALUMINUM CORROSION INHIBITOR STUDY

III.1 Introduction

Aluminum alloys are of primary interest when constructing a heat exchanger due to their combination of high thermal conductivity and low mass. Immersion studies of these alloys in LNH solution with and without the nucleation catalyst likasite revealed limited spotting and localized corrosion on the surface of the aluminum samples. With aluminum being of such high interest, we investigated various corrosion inhibitors which could be used to limit the degradation reactions occurring in the system. In this study, we considered the effectiveness of seven solution-based corrosion inhibitors dissolved in LNH, as well as two coatings applied to the surface of the aluminum [28].

III.2 Materials and Methods

III.2.1 Material Synthesis and Preparation

LNH and likasite were prepared as described in CHAPTER II. Corrosion inhibitors, sodium chromate tetrahydrate (Alfa Aesar, 99+ % purity), lithium molybdate (Sigma Aldrich, 99.9 % purity), cerium nitrate hexahydrate (Alfa Aesar, 99.5% purity), and anhydrous sodium metasilicate (Alfa Aesar, tech. grade) were used as received without further modification. Trivalent (MIL-DTL-5541 Type II, Class 1A) and hexavalent (MIL-DTL-5541 Type I, Class 1A) chromate conversion coatings were applied off-site by a commercial supplier and provided to us for testing. Hexavalent

chromate is highly toxic and has many environmental regulations related to use, including the Restriction of Hazardous Substances Directive (RoHS) issued by the European Union [29]. The trivalent (Type II) coating complies with the RoHS regulations as there is not hexavalent chromate present and is an environmentally safer option.

Table 5. Aluminum Corrosion Inhibitors

Name	ID	Concentration
No Inhibitor	NI	N/A
Lithium Molybdate	LM	10.9 mmol
Lithium Molybdate/Cerium Nitrate	LMCN	10.9 mmol
Sodium Metasilicate	NS	10.9 mmol
Sodium Metasilicate/Cerium Nitrate	NSCN	10.9 mmol
Low Concentration Sodium Chormate	LCNC	10.9 mmol
High Concentration Sodium Chromate	HCNC	32.7 mmol
Cerium Nitrate	CN	10.9 mmol
Hexavalent Chromate Conversion Coating	HCC	Coating
Trivalent Chromate Conversion Coating	TCC	Coating

Solution-based corrosion inhibitors were selected based on: 1) observations suggesting that the corrosion caused by LNH on Al 1016 is effectively inhibited by dissolved lithium chromate [14], and 2) non-chromate inhibitors which were found to be effective at inhibiting corrosion of Aluminum 2024 in sodium chloride solutions. Solution inhibitors were dissolved at concentrations of sodium chromate at 0.1 wt% (10.9 mmol) (LCNC) and 0.3 wt% (32.7 mmol) (HCNC) [14], lithium molybdate (LM), cerium nitrate (CN), and sodium metasilicate (NS) at 10.9 mmol. Additionally, the

combinations of lithium molybdate with cerium nitrate (LMCN) and sodium metasilicate with cerium nitrate (NSCN) be carried out at a concentration of 5.45 mmol for each inhibitor for a total inhibitor concentration of 10.9 mmol [28]. Inhibitors were weighed into borosilicate glass vials and prepared as discussed in the previous chapter. The inhibitors lithium molybdate and sodium metasilicate were not completely soluble in the LNH and some material remained on the bottom of the vials containing these. The trivalent chromate conversion coated (TCC) samples and hexavalent chromate conversion coated (HCC) samples were used as received and placed in vials. Five samples of Al 1100, Al 6061, and Al 4047 were tested with each corrosion inhibitor; three of those samples were immersed in LNH with likasite and two were in pure liquid LNH.

Aging was carried out in an oven set to 50 °C for 6 months, as described previously. All samples were immediately and thoroughly rinsed in DI water after removal from LNH and allowed to dry. The mass of the samples were taken to quantify the mass of surface products observed on many of the samples. Corrosion rates of the aluminum samples immersed in solution based inhibitors were then determined after removal of corrosion products on aluminum samples according to ASTM G1-03, using a concentrated nitric acid solution (sp. gr. 1.42) for 90-120 seconds at room temperature. After the acid soak, aluminum samples were rinsed, sonicated in DI water, and brushed with a non-metallic brush to ensure the removal of corrosion products. Mass loss of the metal samples after cleaning were corrected to a reference sample, which underwent the same cleaning procedure, to minimize error in removal of the non-corroded base metal.

Coated samples did not undergo the acid etching cleaning process, as this would likely lead to removal of the protective coating.

III.2.2 Material Characterization

Optical microscopy was carried out using an Olympus BX53M microscope equipped with an Olympus UC30 camera under bright field reflected light conditions. Differential scanning calorimetry (DSC) was carried out using a TA Instruments Q2000 using N_2 flow gas at 50 $mL \cdot min^{-1}$ and liquid nitrogen cooling. Liquid samples of 8.5 µL were placed in aluminum pans and hermetically sealed. Scans were carried out from -35 °C to 50 °C with a ramp rate of 10 $°C \cdot min^{-1}$.

III.3 Results

The mass gain or loss of aluminum 1100, 6061, and 4047 samples in LNH solutions with corrosion inhibitors are shown in Figure 8. The inhibitors, low concentration sodium chromate, and high concentration sodium chromate significantly reduce the amount of mass gain as compared to those samples with no inhibitor present (NI). This improvement is more pronounced in those samples with likasite present where corrosion has been reduced to near-zero. Lithium molybdate and sodium metasilicate are also good options for limiting corrosion in both neat LNH and with likasite present. However, these inhibitors do lead to a mass gain by deposition of a precipitate on the surface of the aluminum as seen in Figure 9. Lithium molybdate/cerium nitrate, sodium metasilicate/cerium nitrate, and cerium nitrate were shown to be effective in neat LNH, but large corrosion rates were measured in the samples with likasite present. In the case

of Al 1100 in LNH with likasite, an obvious precipitate was observed on the surface of the samples with lithium molybdate/cerium nitrate and sodium metasilicate/cerium nitrate samples, and pits were observed on the surface of the samples with cerium nitrate (Figure 9). From figure 9, it can also be noted that when in contact with cerium nitrate and likasite in LNH the Al 1100, Al 6061, and Al 4047 all have visibly distinct surface corrosion.

Trivalent chromate conversion coating on the aluminum samples effectively limited the mass gain of all three alloys, indicating it effectively limited the corrosion. Hexavalent chromate conversion coating was effective at limiting mass gain, and therefore corrosion with the Al 1100 and Al 4047 samples, but was not effective at limiting the corrosion with the Al 6061 alloy. A layer of corrosion product is easily seen on the surface of these samples (Figure 9 b).

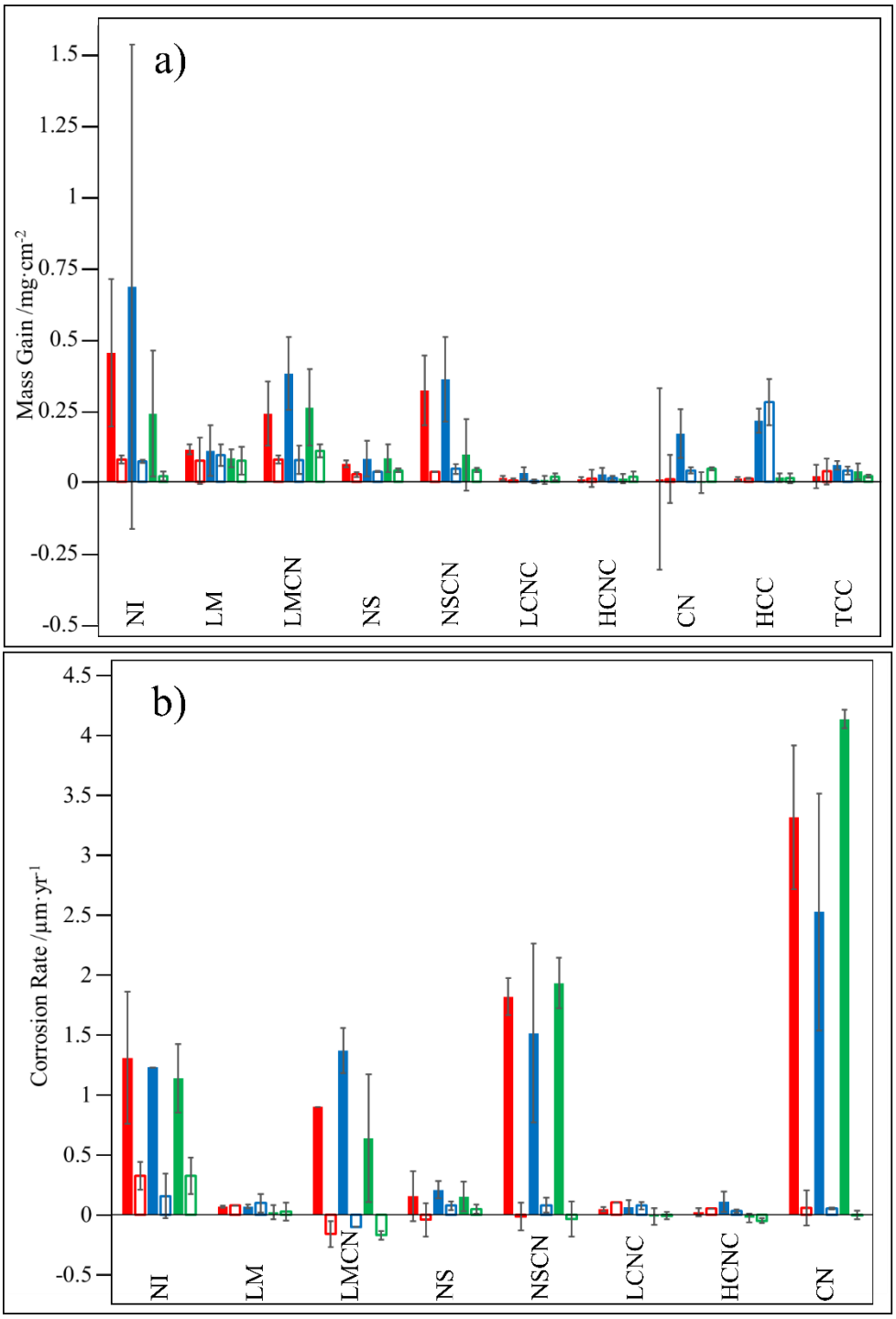

Figure 8. a) Mass gain and b) corrosion rate of aluminum alloys in LNH solutions with inhibitors present. Blue bars are Al 1100, red bars are Al 6061, and green bars are Al 4047. Solid bars represent samples with likasite present, while hollow bars are neat LNH.

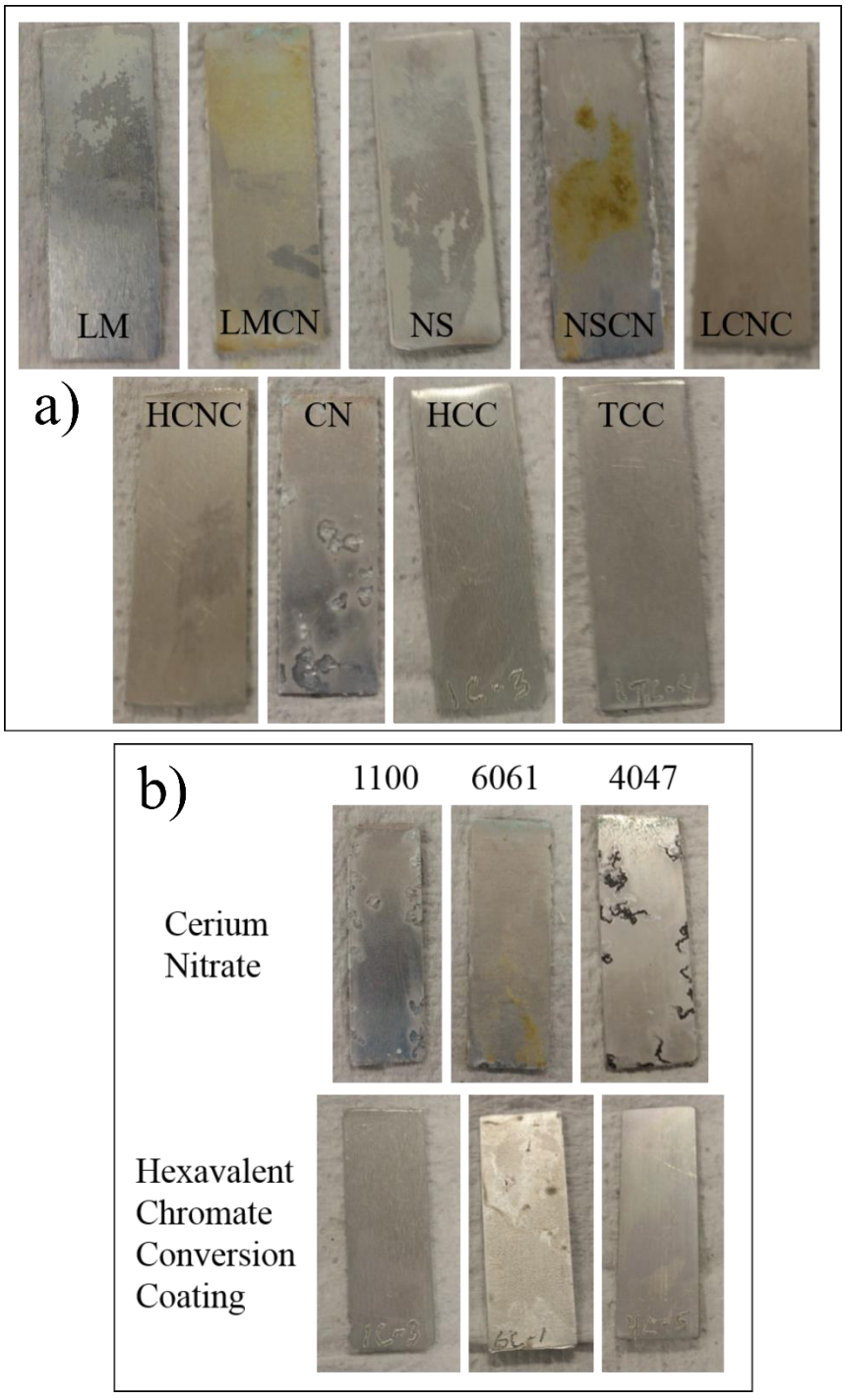

Figure 9. a) Photographs of Al 1100 samples after aging for six months in LNH solution with likasite and the marked inhibitor present. b) Photographs of aluminum alloys after aging in LNH with likasite and inhibitors. Different alloys reacted with the inhibitors in distinctly different manners.

As with the previous study, after six months of aging, the thermal properties of the LNH solutions were tested following previously described methods (Figure 10). Samples were selected as those inhibitors which appeared to perform well in the LNH/likasite solution. The DSC study revealed that melting temperatures of the solutions were slightly depressed. This is expected as thermal analysis of the solution based inhibitors in the LNH carried out prior to the study showed a decrease in melting temperature as the inhibitor concentration increases. The heat of fusion measurements were varied, but generally fall within uncertainty from the accepted value for the heat of fusion of LNH [9]. The upper and lower bounds depicted by the red horizontal lines in Figure 8 are ± 5 °C of the melting temperature and ± 5% of the heat of fusion of LNH; these bounds are intended as visual guides.

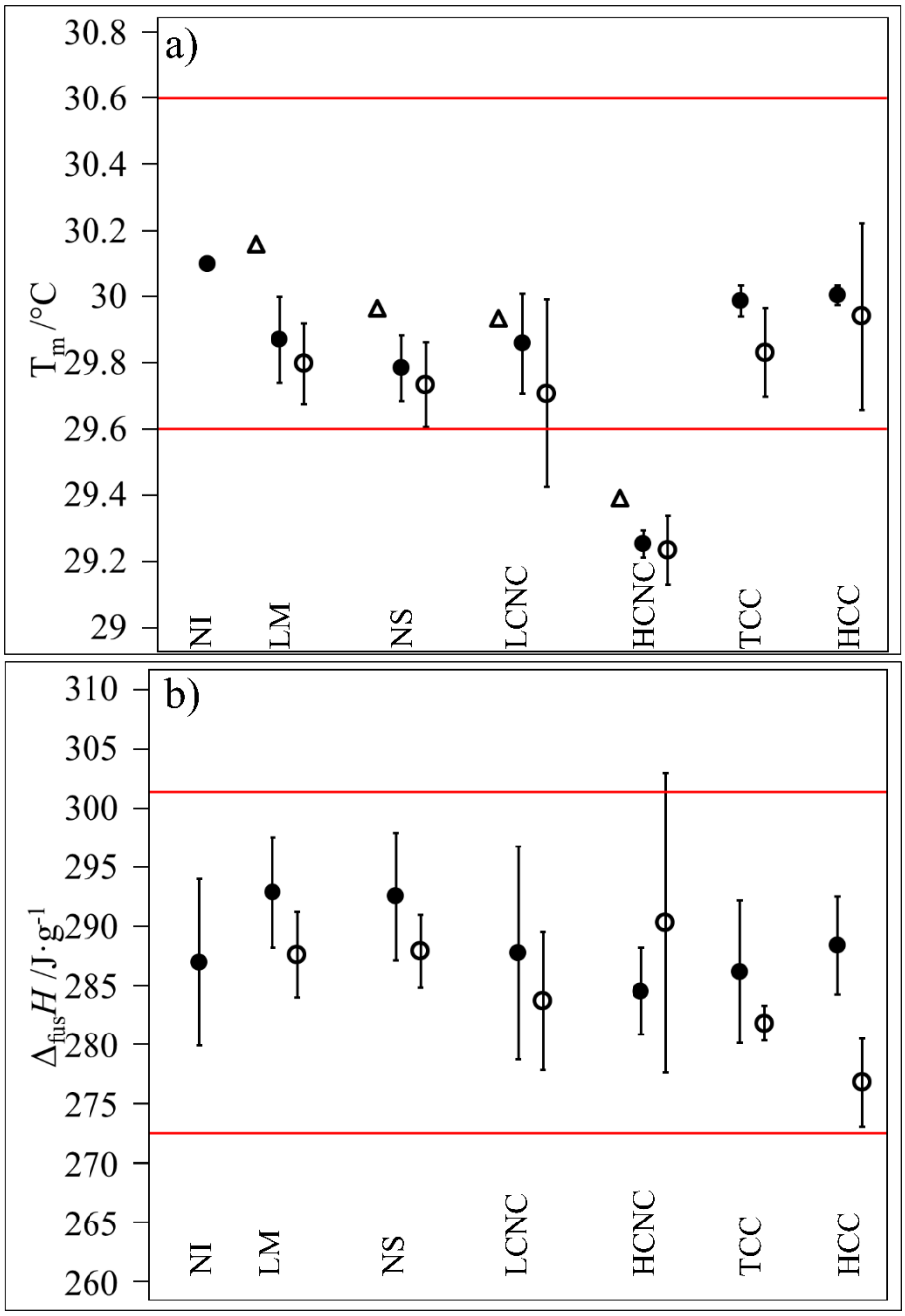

Figure 10. Thermal data for LNH inhibitor solutions after aging. The triangles indicate the melting temperature of LNH with inhibitor solutions before aging. Circles indicate measurements taken after aging; the empty circle symbols indicate neat LNH while the filled circle symbols are samples with likasite present. a) Shows the melting temperature of LNH while b) shows the heat of fusion. Error bars represent a 2σ standard deviation between samples.

III.4 Discussion

The mass gain evident on aluminum samples in lithium molybdate/cerium nitrate and sodium metasilicate/cerium nitrate added to LNH with likasite was due to a thick, densely deposited precipitate on the surface of the aluminum samples. Lithium molybdate and sodium metasilicate also had obvious surface deposits, though to a lesser extent. Cerium nitrate added to LNH with likasite present resulted in pits forming on the Al 1100 and 4047 samples, and a yellow film similar that seen with the lithium molybdate/cerium nitrate and sodium metasilicate/cerium nitrate inhibitors. Deposition of a thick film on the aluminum surface, even if little corrosion is observed, could hinder heat transfer between LNH and the aluminum surface, decreasing the rate of heat transfer by the PCM significantly. If these materials were to be pursued for use, further studies would need to be done on metallic samples after aging to the additional interfacial resistance added by the precipitate layer. Degradation of the two corrosion inhibitor coatings (trivalent chromate conversion coating and hexavalent chromate conversion coating) was quantified using overall mass gain, combined with microscopic and visual observation. Of these coatings, hexavalent chromate conversion coating showed improvement over the uninhibited cases for Al 1100 and Al 4047, but was not as effective in inhibiting corrosion in the Al 6061 case as evident by not only the mass gain, but also the visual observation of localized corrosion on the surface of the samples. The coating may not have adhered as well or been as thick after application as the other alloys tested. Trivalent chromate conversion coating was effective at limiting the mass gain for all of the aluminum alloys tested.

The corrosion rates of the aluminum corrosion inhibitor study followed the previously mentioned trend of corrosion rates being greater in cases where likasite is present. Most notably are those cases which have cerium nitrate as an intended corrosion inhibitor. The cerium nitrate amplifies the corrosive effect of the likasite, actually leading to increased corrosion, making this a nonviable option for LNH/likasite solutions. Lithium molybdate, sodium metasilicate, low concentration sodium chromate, and high concentration sodium chromate reduce the corrosion rate significantly from the original severity. As low concentration sodium chromate and high concentration sodium chromate both limit the corrosion effectively, it can be recommended that the lower concentration be used to limit melting point depression observed in the thermal studies.

Corrosion is limited by chromate conversion coatings through creation of a barrier preventing LNH from coming into direct contact with the aluminum. During application, the coatings form a thin layer of complex oxides on the surface of the aluminum, protecting it from attack [25]. The solution based inhibitors will also protect the aluminum samples by forming a protective layer on the surface of the aluminum. Molybdates, and chromates form passive protective adsorbed layers on the surface of the aluminum samples which act primarily as a barrier to prevent corrosion, while silicates are anodic inhibitors which will form a layer which electrochemically acts to protect the base aluminum[14, 25].

III.5 Conclusion

Aluminum is a highly desirable material for use in heat exchangers, but undergoes corrosion when in contact with LNH (with or without likasite present). To limit the corrosion of the aluminum alloys, lithium molybdate, sodium metasilicate, or sodium chromate may be added in low concentration to the LNH/likasite solution. Additionally, aluminum that is going to be in contact with LNH/likasite may be coated with a trivalent chromate conversion coating to effectively limit corrosion.

The corrosion rate with likasite present in the LNH is significantly higher and more severe when considering inhibitors with cerium nitrate present. Corrosion rates for aluminum with lithium molybdate, sodium metasilicate, sodium chromate, or trivalent chromate conversion coating present are near-zero, and there is no increase in corrosion rate observed when likasite is present. The hexavalent chromate conversion coating is effective at limiting corrosion with Al 1100 and Al 4047 both in the presence of likasite and in the neat LNH, however it was not effective when applied to the Al 6061 in either solution. The thermal data shows that the LNH with likasite and inhibitors present is a stable solution for at least six months and does not undergo degradation of thermal properties.

CHAPTER IV

SUMMARY

The large specific and volumetric enthalpies of fusion and near-room temperature melting point of lithium nitrate trihydrate (LNH) make it a promising material for heat exchanger development. In this study we examined the corrosive effects of LNH on common heat exchanger materials including nine polymeric materials and twelve metallic alloys. Nylon, PVC and fluorinated polymers performed well in the LNH solutions, with no degradation observed, and can be recommended for use in heat exchanger systems. Of the metallic alloys, copper and aluminum alloys were corroded by the LNH solutions, however the stainless steels, nickel alloy, and titanium alloys were found to be compatible with LNH and can be recommended for use as no corrosion was observed. Aluminum alloys were of particular interest when considering heat exchanger construction, so we investigated possible corrosion inhibitors to limit the damaging effects of the LNH solution. It was found that corrosion of aluminum alloys could be mitigated by dissolving low concentrations of lithium molybdate, sodium metasilicate, or sodium chromate directly into LNH, or a trivalent chromate conversion coating may be applied to the surface of the aluminum. We can recommend aluminum as a construction material for high cooling power energy storage modules containing LNH if these inhibitors are present.

REFERENCES

[1] Hale DV, Hoover MJ, Oneill MJ. Phase Change Materials Handbook. NASA CR-61363. Huntsville, AL: Lockheed Missiles & Space Company; 1971.

[2] Humphries WR, Griggs EI. A Design Handbook for Phase Change Thermal Control and Energy Storage Devices. Huntsville, AL1977.

[3] Mehling H, Cabeza LF. Heat and cold storage with PCM : an up to date introduction into basics and applications. Harald Mehling, Luisa F. Cabeza: Berlin : Springer, [2008]; 2008.

[4] Zalba B, Marín JM, Cabeza LF, Mehling H. Review on thermal energy storage with phase change: materials, heat transfer analysis and applications. Applied Thermal Engineering. 2003;23:251-83.

[5] Lane GA. Solar heat storage : latent heat materials. editor, George A. Lane: Boca Baton, Fla. : CRC Press, [1983-]; 1983.

[6] Jankowski NR, McCluskey FP. A review of phase change materials for vehicle component thermal buffering. Applied Energy. 2014;113:1525-61.

[7] Economou JT. Electrification of aircraft systems: Power and control. Proceedings of the Institution of Mechanical Engineers Part G-Journal of Aerospace Engineering. 2013;227:577-.

[8] Sharma A, Tyagi VV, Chen CR, Buddhi D. Review on thermal energy storage with phase change materials and applications. Renewable and Sustainable Energy Reviews. 2009;13:318-45.

[9] Shamberger PJ, Reid T. Thermophysical Properties of Lithium Nitrate Trihydrate from (253 to 353) K. Journal of Chemical and Engineering Data. 2012;57:1404-11.

[10] Shamberger PJ, Reid T. Thermophysical Properties of Potassium Fluoride Tetrahydrate from (243 to 348) K. Journal of Chemical and Engineering Data. 2013;58:294-300.

[11] Shamberger PJ, O'Malley MJ. Heterogeneous nucleation of thermal storage material LiNO3·3H2O from stable lattice-matched nucleation catalysts. Acta Materialia. 2015;84:265-74.

[12] Hoover M, Grodzka PG, O'Neill M. Space Thermal Control Development. Huntsville, AL: Lockheed Missiles & Space Company; 1971.

[13] MatWeb Material Property Data. http://wwwmatwebcom/. Accessed Dec. 2016.

[14] Luo CH. Corrosion of Aluminium in Concentrated LiNO3 Solution at High Temperature. International Journal of Electrochemical Science. 2015;10:4706-17.

[15] Pizzolato PJ, Farmer R. Phase Change Thermal Control Development. NASA Technical Summary Report. 1973;NASA-CR-161994.

[16] Cabeza LF, Roca J, Nogues M, Mehling H, Hiebler S. Immersion corrosion tests on metal-salt hydrate pairs used for latent heat storage in the 48 to 58 degrees C temperature range. Materials and Corrosion-Werkstoffe Und Korrosion. 2002;53:902-7.

[17] Gawron K, Schröder J. Properties of some salt hydrates for latent heat storage. International Journal of Energy Research. 1977;1:351-63.

[18] Cabeza LF, Illa J, Roca J, Badia F, Mehling H, Hiebler S, et al. Middle term immersion corrosion tests on metal-salt hydrate pairs used for latent heat storage in the 32 to 36 degrees C temperature range. Materials and Corrosion-Werkstoffe Und Korrosion. 2001;52:748-54.

[19] Sole A, Miro L, Barreneche C, Martorell I, Cabeza LF. Corrosion of metals and salt hydrates used for thermochemical energy storage. Renewable Energy. 2015;75:519-23.

[20] Moreno P, Miró L, Solé A, Barreneche C, Solé C, Martorell I, et al. Corrosion of metal and metal alloy containers in contact with phase change materials (PCM) for potential heating and cooling applications. Applied Energy. 2014;125:238-45.

[21] Heard CL, Ayala R. Carbon and stainless steel in solutions of lithium nitrate in ammonia at moderate temperatures. Materials and Corrosion-Werkstoffe Und Korrosion. 2003;54:609-11.

[22] Yoder CH, Bushong E, Liu X, Weidner V, McWilliams P, Martin K, et al. The synthesis and solubility of the copper hydroxyl nitrates: gerhardtite, rouaite and likasite. Mineralogical Magazine. 2010;74:433-40.

[23] Thiel JP, Chiang CK, Poeppelmeier KR. STRUCTURE OF LIAL2(OH)7.2H2O. Chemistry of Materials. 1993;5:297-304.

[24] Nguyen TH, Foley RT. The Chemical Nature of Aluminum Corrosion: III . The Dissolution Mechanism of Aluminum Oxide and Aluminum Powder in Various Electrolytes. Journal of The Electrochemical Society. 1980;127:2563-6.

[25] Vargel C. Corrosion of aluminium. 1st ed. Christian Vargel ; foreword by Michel Jacques ; translated by Martin P. Schmidt. 2004.

[26] Obot IB, Obi-Egbedi NO, Umoren SA, Ebenso EE. Synergistic and Antagonistic Effects of Anions and Ipomoea invulcrata as Green Corrosion Inhibitor for Aluminium Dissolution in Acidic Medium. International Journal of Electrochemical Science. 2010;5:994-1007.

[27] Francis R. The corrosion of copper and its alloys : a practical guide for engineers. Roger Francis: Houston, Tex. : NACE International, ©2010.; 2010.

[28] Taylor SR, Chambers BD. Identification and characterization of nonchromate corrosion inhibitor synergies using high-throughput methods. Corrosion. 2008;64:255-70.

[29] Directive 2011/65/EU of the European Parliament and of the Council of 8 June 2011 on the restriction of the use of certain hazardous substances in electrical and electronic equipment (recast).

APPENDIX

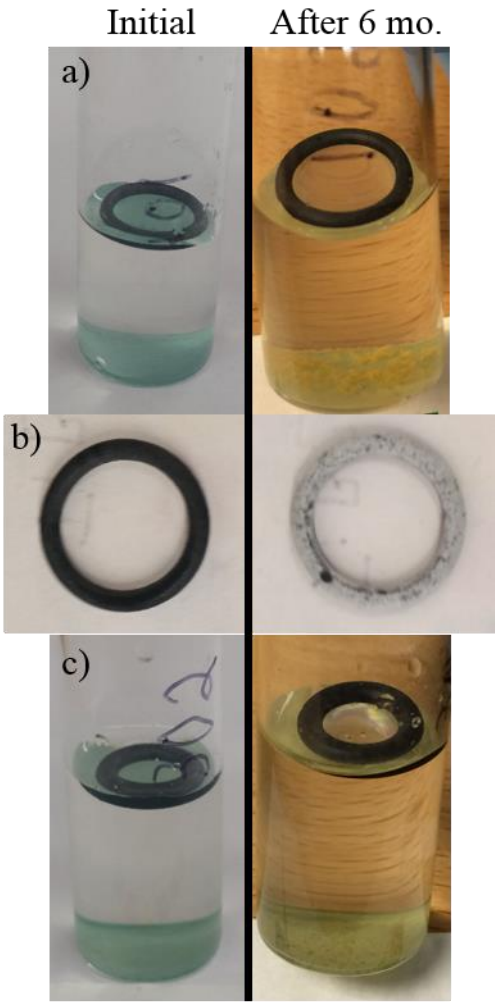

Figure A1. Photographs of the initial and final condition of a) vails containing EPDM O-rings, b) EPDM O-rings, c) vials containing BNR O-rings.

Table A1. Mass change and swelling of polymer samples.

Sample	mean/mg·mm^{-2}	2s/mg·mm^{-2}	Mean % Change OD	2s	Mean % Change ID	2s	Mean % Change Thickness	2s
EPDM	$-1.44\cdot10^{-3}$	$8.3\cdot10^{-4}$	-0.17	0.6	0.06	2.1	-1.50	1.0
Nylon	$4.46\cdot10^{-5}$	$9.6\cdot10^{-5}$	3.02	7.4	0.05	2.2	0.21	0.2
BNR	$-1.48\cdot10^{-3}$	$1.2\cdot10^{-4}$	-0.21	1.9	-1.87	2.8	1.80	0.6
VMQ	$-8.34\cdot10^{-4}$	$4.9\cdot10^{-4}$	0.50	1.3	-1.10	1.0	-2.20	0.3
FKM	$4.81\cdot10^{-4}$	$1.0\cdot10^{-4}$	-0.47	0.1	-0.42	0.2	-0.70	0.2
PTFE	$6.49\cdot10^{-5}$	$2.7\cdot10^{-4}$	0.22	0.2	0.37	0.3	-4.07	1.4
FVMQ	$1.30\cdot10^{-4}$	$1.0\cdot10^{-4}$	-0.12	0.2	0.75	0.1	-0.59	1.7
Sample	mean/mg·mm^{-2}	2s/mg·mm^{-2}	Mean % Change Length	2s	Mean % Change Width	2s	Mean % Change Thickness	2s
PVC	$8.14\cdot10^{-5}$	$8.1\cdot10^{-5}$	0.17	0.3	0.43	0.2	2.61	0.7
PC	$1.28\cdot10^{-4}$	$1.3\cdot10^{-5}$	0.23	0.1	0.52	1.0	4.61	1.4

N = 2 for all calculations

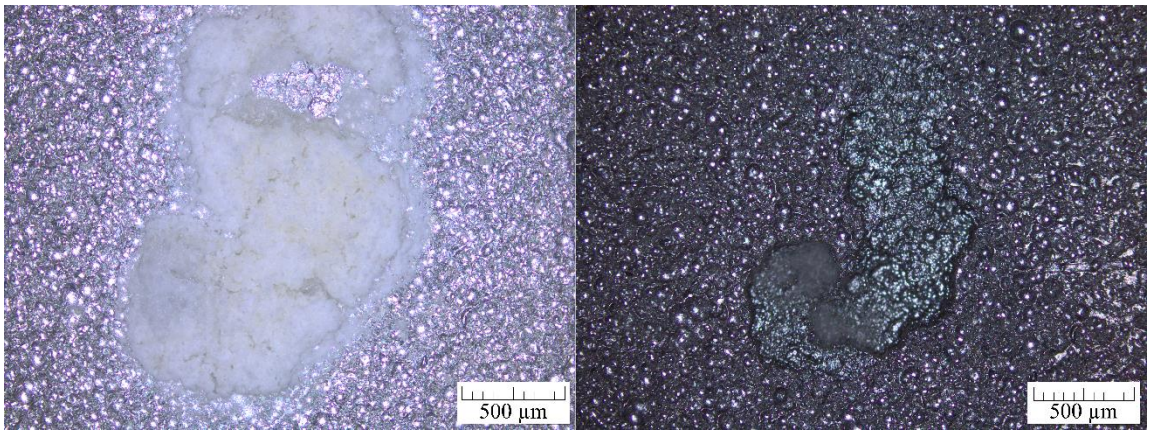

Figure A2. Microscopy images of the Al 1100 localized corrosion spots before and after cleaning.